ACS OMEGA

Open Access

http://pubs.acs.org/journal/acsodf

Article

The Novel Long-Acting Peptide S6-FA Attenuates Liver Fibrosis In Vitro and In Vivo

Mingmin Li,[⊥] Liang Qi,[⊥] Jin Huang, Haonan Li, Wei Cheng, Zihan Shi, Xianxing Jiang,* Yifeng Zhou,* and Wanxiang Jiang*

Cite This: *ACS Omega* 2025, 10, 9661−9674

Read Online

ACCESS | Metrics & More | Article Recommendations | Supporting Information

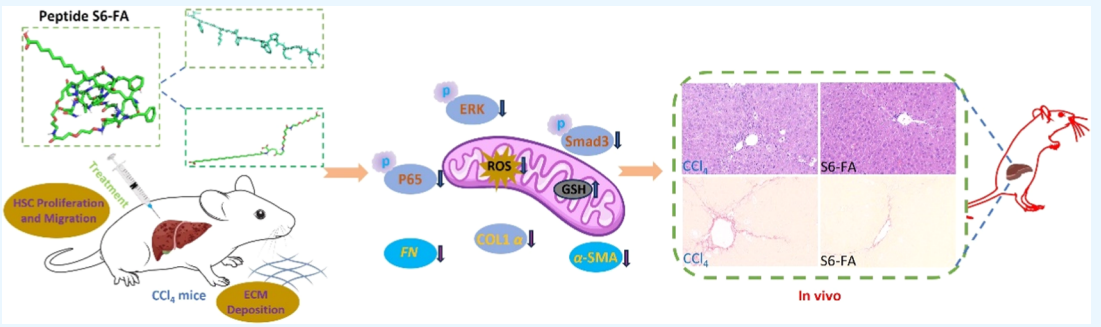

ABSTRACT: Liver fibrosis can progress to cirrhosis and hepatocellular carcinoma. Currently, there is no effective drug for liver fibrosis. The peptide 6 (T6) is an endogenous peptide derived from human intrauterine adhesion tissues and has antifibrotic potential. Here, to improve the long-term efficacy and activity of T6, we conducted the rational modified of T6 through studying structure−activity, and synthesized a series of analogues. Among them, S6 and S6-FA exhibited optimal antihepatic fibrosis activity, and S6-FA had a stronger long-acting effect than T6 and S6. The two analogues inhibited the expression of α-SMA and Collagen 1 in TGF-β-induced LX2 cells model and CCl_4-induced mouse model of liver fibrosis. Besides, we discovered that S6 and S6-FA remarkably reduced the AST and ALT serum levels. Mechanistic studies have demonstrated that analogues inhibited liver fibrosis through inhibiting Erk, Smad and P65 pathways. This study provided that the novel peptide S6 and S6-FA is potential candidate compounds for treating liver fibrosis.

INTRODUCTION

Liver fibrosis is a pathological change in the process of chronic liver disease, primarily characterized by the excessive deposition of extracellular matrix (ECM) produced by activated hepatic stellate cells (HSCs), leading to alterations in liver structure and functional impairment.[1−4] The occurrence and development of liver fibrosis are associated with various factors, such as chronic viral hepatitis, alcoholic liver disease, nonalcoholic fatty liver disease, and autoimmune hepatitis.[5,6] If liver fibrosis persists, the necrosis and apoptosis of normal liver parenchymal cells lead to the continuous accumulation of extracellular matrix, eventually forming cirrhosis, and may even cause portal hypertension or liver cancer, leading to liver failure.[1,7] Hence, it represents an important stage in the progression of various chronic liver diseases to cirrhosis.[8] It has been reported that approximately 1% of the global population is affected by liver fibrosis, resulting in more than 2 million deaths worldwide due to complications related to fibrosis/cirrhosis.[9,10] Currently, it is of immediate importance to identify effective agents for the treatment of liver fibrosis.

As key biological mediators, peptides have been widely used in the treatment of a variety of diseases, including cancer, diabetes, osteoporosis, multiple sclerosis, HIV infection and chronic pain, because of their remarkable activity, high selectivity and low toxicity.[11,12] Therefore, there are many bioactive peptides in preclinical studies with potential to treat fibrosis.[13,14] Ac-SDKP, an endogenous short peptide produced by the continuous hydrolysis of thymosin β4 through endopeptidase-α and prolyl oligo-peptidase, has a negative regulatory role in the development of liver fibrosis.[15] Recombinant truncated latency-associated peptide alleviates liver fibrosis by inhibiting TGF-β/Smad pathway.[16] Recently, Ying and co-workers found that the peptide 6 (T6) (peptide sequence: TFGGAPGFPLGSPLSSVFPR), an endogenous peptide in patients intrauterine adhesion tissues, which inhibited the cell fibrosis in TGF-β1-induced human endometrial stromal cell line and primary human endometrial stromal cell.[17] TGF-β is a

Received: December 3, 2024
Revised: February 9, 2025
Accepted: February 13, 2025
Published: February 27, 2025

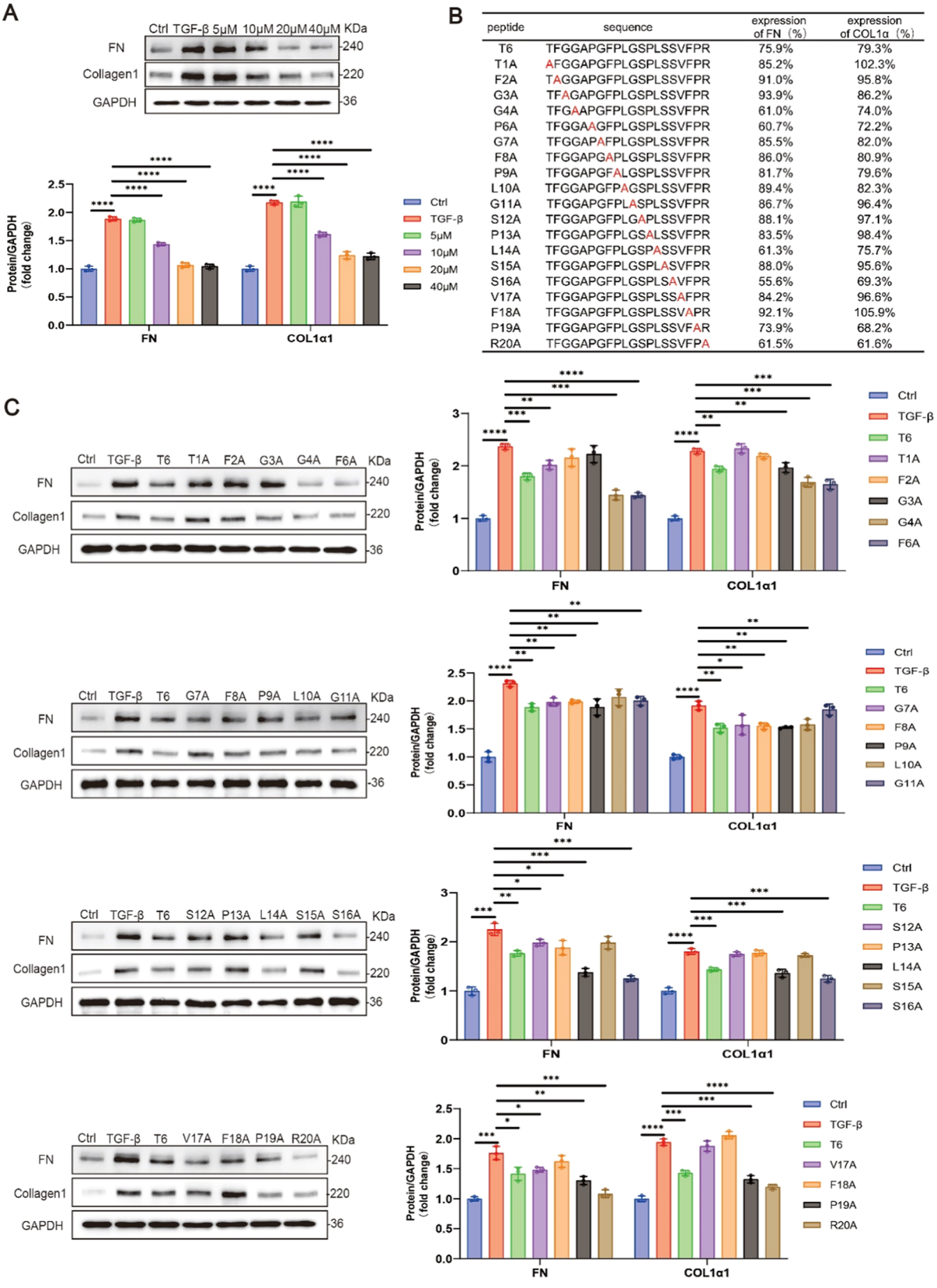

peptide	sequence	expression of FN (%)	expression of COL1α (%)
T6	TFGGAPGFPLGSPLSSVFPR	75.9%	79.3%
T1A	AFGGAPGFPLGSPLSSVFPR	85.2%	102.3%
F2A	TAGGAPGFPLGSPLSSVFPR	91.0%	95.8%
G3A	TFAGAPGFPLGSPLSSVFPR	93.9%	86.2%
G4A	TFGAAPGFPLGSPLSSVFPR	61.0%	74.0%
P6A	TFGGAAGFPLGSPLSSVFPR	60.7%	72.2%
G7A	TFGGAPAFPLGSPLSSVFPR	85.5%	82.0%
F8A	TFGGAPGAPLGSPLSSVFPR	86.0%	80.9%
P9A	TFGGAPGFALGSPLSSVFPR	81.7%	79.6%
L10A	TFGGAPGFPAGSPLSSVFPR	89.4%	82.3%
G11A	TFGGAPGFPLASPLSSVFPR	86.7%	96.4%
S12A	TFGGAPGFPLGAPLSSVFPR	88.1%	97.1%
P13A	TFGGAPGFPLGSALSSVFPR	83.5%	98.4%
L14A	TFGGAPGFPLGSPASSVFPR	61.3%	75.7%
S15A	TFGGAPGFPLGSPLASVFPR	88.0%	95.6%
S16A	TFGGAPGFPLGSPLSAVFPR	55.6%	69.3%
V17A	TFGGAPGFPLGSPLSSAFPR	84.2%	96.6%
F18A	TFGGAPGFPLGSPLSSVAPR	92.1%	105.9%
P19A	TFGGAPGFPLGSPLSSVFAR	73.9%	68.2%
R20A	TFGGAPGFPLGSPLSSVFPA	61.5%	61.6%

Figure 1. Characterization of the peptides. (A) Western blot analysis of FN and COL1α1 expression level in TGF-β-induced LX2 cells treated with different concentrations of peptide T6 ($n = 3$). (B) Alanine scanning mutagenesis of T6 and corresponding peptides against inhibited the expression of FN and COL1α1, as measured by Western blot assay. (C) Western blot analysis of FN and COL1α1 expression in a TGF-β-induced cell model treated with 10 μM analogues ($n = 3$). Data are represented as mean ± SEM *$P < 0.05$, **$P < 0.01$, ***$P < 0.001$ and ****$P < 0.0001$. All compounds are >95% pure by HPLC analysis.

https://doi.org/10.1021/acsomega.4c10956
ACS Omega 2025, 10, 9661−9674

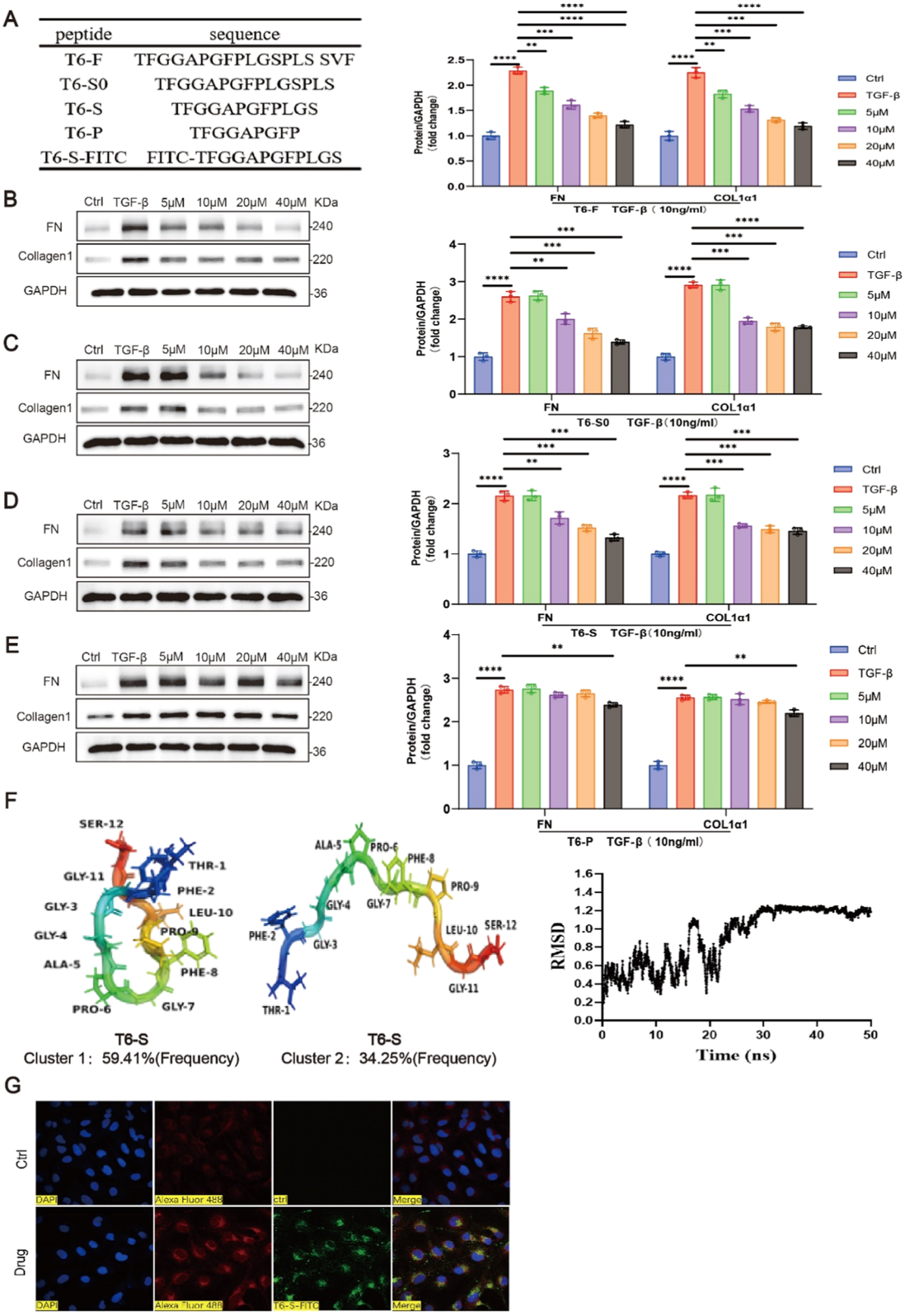

Figure 2. Analysis of the properties of truncated peptides and the conformation of T6-S. (A) Names and sequences of truncated peptides. (B-E) Western blot analysis of FN and COL1α1 expression level in TGF-β-induced LX2 cells treated with different concentrations of short peptide (n = 3). (F) Optimal structures of T6-S in water generated from MD simulations. (G) Peptide T6-S targeting mitochondrial membrane for fluorescence confocal microscopy. Data are represented as mean ± SEM $^{**}P < 0.01$, $^{***}P < 0.001$ and $^{****}P < 0.0001$. All compounds are >95% pure by HPLC analysis.

https://doi.org/10.1021/acsomega.4c10956
ACS Omega 2025, 10, 9661−9674

promoter of fibrotic diseases via activating HSCs and liver fibrogenesis.[18] Therefore, we asked whether T6 could have a functional impact on liver fibrosis.

The main problems in the development of peptides include poor stability, short half-life, high plasma clearance and low drug formation.[19] In order to overcome the above drawbacks, scientists have developed a number of peptide modification strategies, including natural or unnatural amino acid substitutions, C-terminal amidation, cyclization, fatty acid modification.[20] An earlier study has demonstrated that exchanged the lysine at position 29 of the B chain of insulin with the proline residue to obtain the modifier, which can reduce the stability of the oligomeric form and make insulin dissociate more quickly and enter the circulation system to achieve the therapeutic effect.[21] The amino acid Ala at position 8 of semaglutide was replaced by an unnatural α-aminobutyric acid (Aib) amino acid to avoid DPP-4 degradation.[22] Recently, Tina et al. reported that BI,[23] which is a novel GCGR/GLP-1R dual agonist that containing a C18 fatty acid to extend half-life.[24,25] In addition, cyclic peptides are also one of the effective ways to delay the half-life of peptides.[26,27] Here, we modified the linear peptide T6 to enhance its activity and stability.

In the current study, we performed the alanine amino acid scanning experiments to clarify the influence of each amino acid residue of T6 on its antihepatic fibrosis activity, and then synthesized novel analogs. Based on the key sites identified by alanine scanning, we made a truncated modification of T6 and found that the truncated peptide **T6-S** still retained activity. Subsequently, **T6-S** was modified by natural or unnatural amino acid substitutions and C-terminal amidation strategies to improve its stability and activity. Of all the analogues, S6 had the best inhibitory effects of liver fibrosis in TGF-β-induced LX2 cells model. Fatty acid modification can stabilize the peptide structure and improve its stability, thereby prolonging the half-life of peptide drugs.[28] So, we modified **S6** with fatty acids to obtain the analogue **S6-FA**. Furthermore, we investigated the antifibrotic effects and mechanisms of **S6** and **S6-FA** in vitro and in vivo.

RESULTS

Alanine Scanning and C-terminal Truncation. As a starting point for our study, we synthesized the known **T6** peptide to investigate its antiliver fibrosis efficacy on the domain of the fibrinogen protein. First, cell growth was assessed with treatment of T6 at various concentrations by the CCK-8 assay, where we observed that even at a high concentration (64.0 μM), T6 did not affect the growth of LX2 cells (Figure S1C,D). Hepatic stellate cells (HSCs) produce extracellular matrix (ECM) proteins and play a crucial role in the occurrence and progression of liver fibrosis, so we cocultured LX2 cells with TGF-β to induce the expression of fibronectin (FN, a biomarker of HSC activation) and type I collagen (COL1α1, a biomarker of ECM accumulation).[2,29] In the LX2 cell model, FN and COL1α1 expression increased correspondingly after 24 h of TGF-β induction at a concentration of 10 ng/mL. Therefore, we used the TGF-β induced LX2 cell model in our study to evaluate the antifibrotic effects of the fibrinogen domain peptide. Next, we evaluated the dose-dependent effects of T6, showing that T6 dose-dependently affected the expression of FN and COL1α1 (Figure 1A). Therefore, we selected a concentration of 10 μM as the optimal dose for subsequent cell assays.

To precisely identify the specific amino acid residues in peptide T6 that are crucial for its antifibrotic activity, an alanine scanning experiment was carried out, and the inhibitory capacity of T6 on the expression of FN and COL1α1 in LX2 cells was profoundly analyzed and evaluated (Figure 1B). As shown in Figure 1C, the substitution of Thr^1, Phe^2, Ser^{12}, Pro^{13}, Ser^{15}, and Phe^{18} with alanine led to an elevation in the expression levels of FN and COL1α1 for peptides T1A, F2A, S12A, P13, S15A, and F18A. In contrast, the replacement of Gly^3, Leu^{14}, and Pro^{19} with alanine merely impacted the expression of FN, while exerting no effect on the expression of COL1α1. Intriguingly, however, the expression levels of FN and COL1α1 for peptides G7A, F8A, P9A, and L10A were nearly identical to those of the control group, suggesting that Gly^7-Phe^8-Pro^9-Leu^{10} might be a key and conserved site for the antifibrotic activity of T6. The substitution of Gly^4, Phe^6, Leu^{14}, Ser^{16}, Pro^{19}, and Arg^{20} with alanine resulted in a marginally higher inhibitory activity against FN and COL1α1 compared to with alanine resulted in a marginally higher inhibitory activity against FN and COL1α1 compared to the parent peptide, suggesting that these six residues might not significantly influence the activity. Notably, the replacement of Gly^4 and Pro^6 with alanine significantly augmented the inhibitory activity, suggesting that these two residues might be amenable to further optimization. In conclusion, the alanine scanning study of peptide T6 discloses the possibility of further structural optimization.

In light of the high degree of conservation at the N-terminus and the crucial role of the C-terminal region in antifibrotic activity, we meticulously designed and successfully synthesized four truncated derivatives of the T6 C-terminal peptides, designated as compounds **T6-F**, **T6-S0**, **T6-S**, and **T6-P** (Figure 2A). It was discovered that when **T6-F**, **T6-S0**, and **T6-S** were administered to LX2 cells at a concentration of 10 μM in response to TGF-β, they were capable of effectively suppressing the activity of FN and COL1α1 (Figure 2B−D). Nevertheless, surprisingly, **T6-P** lost its activity at a concentration of 10 μM and merely exhibited lower activity at a concentration of 40Mm (Figure 2E). These results further validate that truncating the C-terminal sequence of the parental peptide to position 10 and retaining Gly^7-Phe^8-Pro^9-Leu^{10} does not impact the peptide's ability to inhibit the activity of FN and COL1α1. This finding offers a novel perspective for comprehending the significance of amino acid residues in the C-terminal region in antifibrotic activity. Among the truncated peptides, we prioritized the further optimization of peptide **T6-S** because it is smaller in size compared to T6 and has a comparable inhibitory efficiency in ECM protein synthesis in cells.

To further optimize the peptide **T6-S**, we employed molecular dynamics (MD) simulations to dissect the conformation of **T6-S** in water (Figure 2F). The equilibrium time for **T6-S**, water, and ions was set at 50 ns, the temperature at 300 K, and the Cpptraj module within the Amber16 software package was utilized to analyze the molecular dynamics trajectories. The RMSD results show that the simulation trajectory in the 10−50 ns interval is stable enough; therefore, such a simulation interval was chosen for the simulation trajectory. We found that T6-S presented two different linear conformations.[30]

It has been demonstrated that one of the crucial roles of IFs within animal cells is to guarantee the normal operation of mitochondria.[31,32] Desmin, a core constituent of the IF network in muscle cells, serves as a paradigmatic example in regulating mitochondria-related factors.[33,34] A multitude of pathological conditions (collectively referred to as desminopathies) are triggered by mutations in Desmin, resulting in aberrant

https://doi.org/10.1021/acsomega.4c10956
ACS Omega 2025, 10, 9661−9674

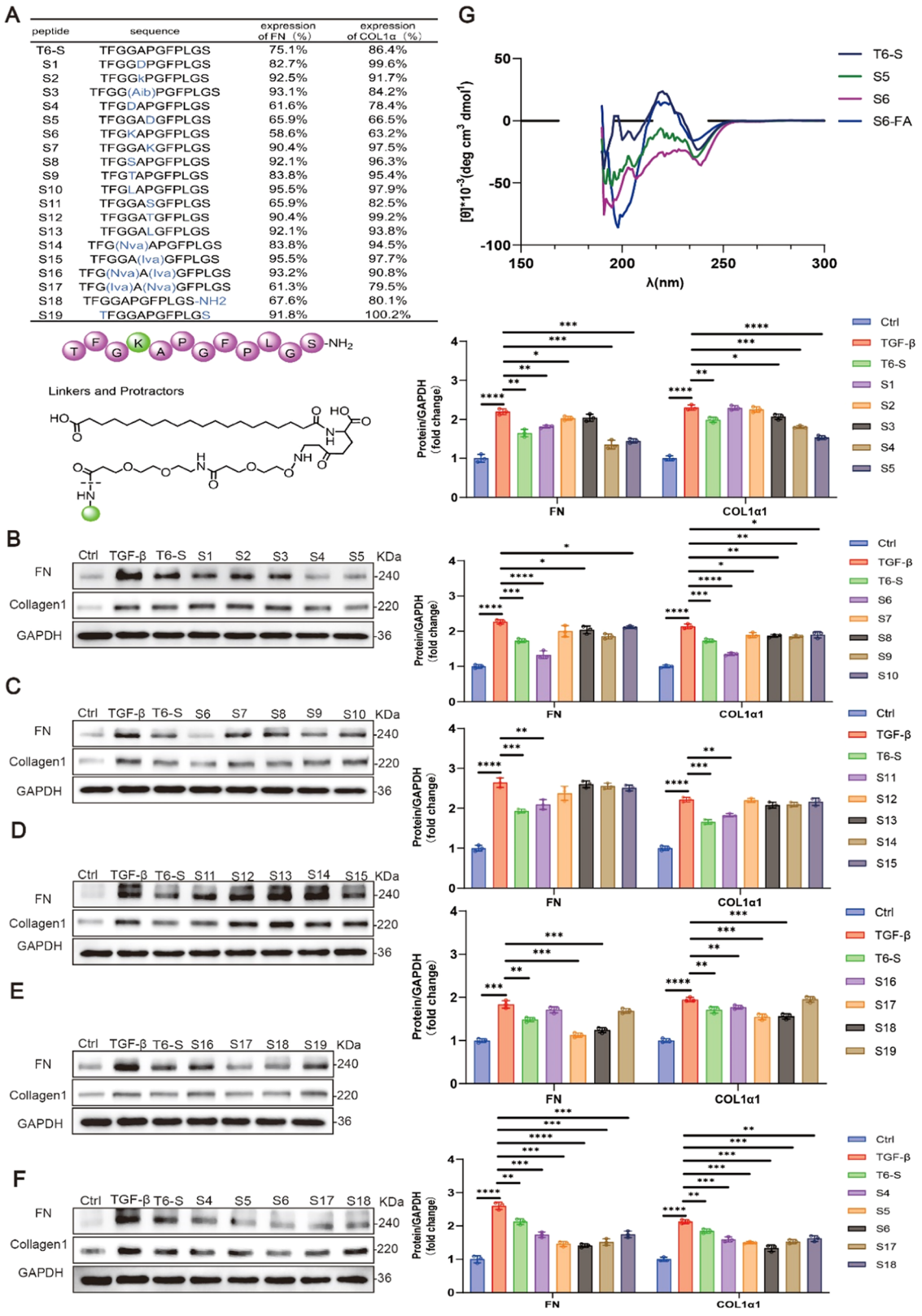

Figure 3. Characterization of the peptides. (A) Inhibition of FN and COL1α1 expression in LX2 cells as determined by Western blot analysis ($n = 3$). (B-E) The modifications of maternal peptide T6-S and the antifibrosis effect of S1−S19 peptides in vitro ($n = 3$). (F) Intensive screening of modified peptides for enhanced therapeutic effects, with detection of FN and COL1α1 expression ($n = 3$). (G) CD spectra of T6-S, S5, S6 and S6-FA in 50% trifluoroethanol (TFE) aqueous solution. Data are represented as mean ± SEM $^*P < 0.05$, $^{**}P < 0.01$, $^{***}P < 0.001$ and $^{****}P < 0.0001$. All compounds are >95% pure by HPLC analysis.

distribution and morphology of mitochondria, as well as compromised mitochondrial respiratory function.[35,36] These data imply that the interaction with Desmin constitutes a necessary prerequisite for the normal functionality of

https://doi.org/10.1021/acsomega.4c10956
ACS Omega 2025, 10, 9661−9674

Scheme 1. Synthesis of Peptides T6-S[α]

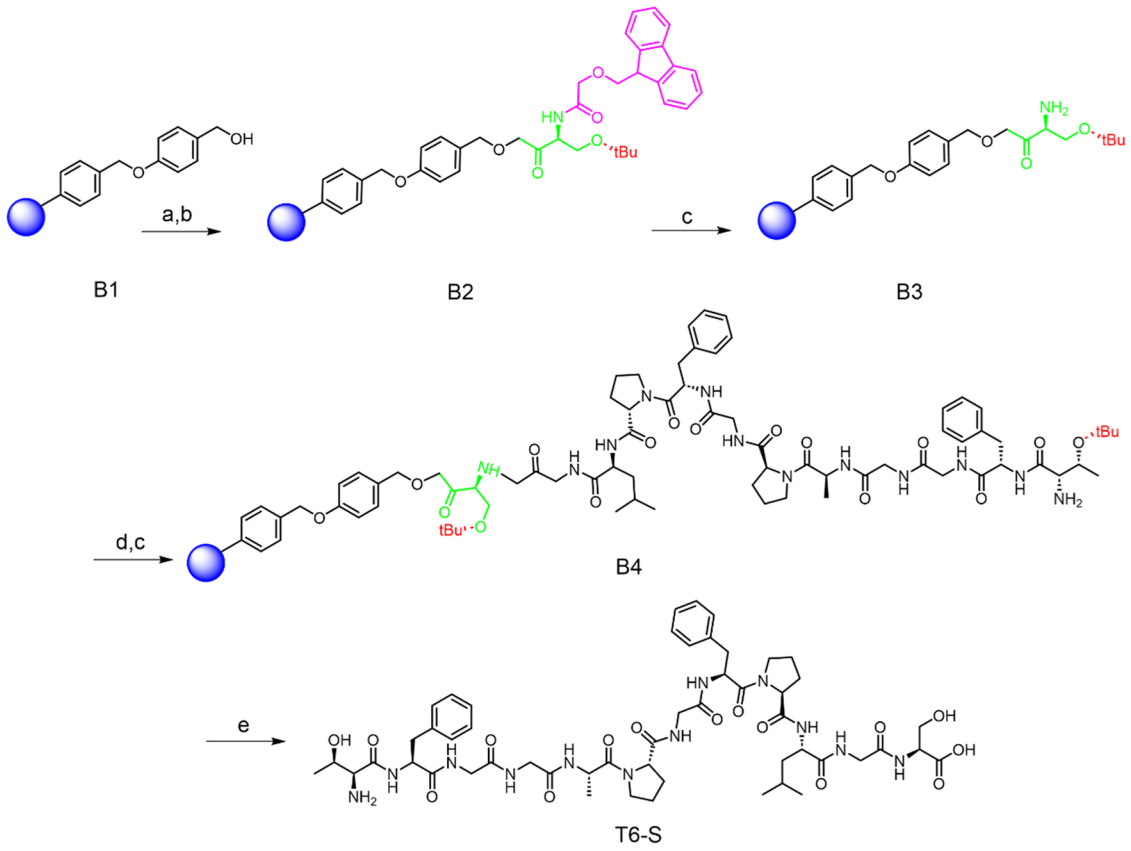

[α]Reagents and conditions: (a) N,N-dimethylformamide (DMF) + dichloromethane (DCM), 25 °C, 0.5 h. (b) Fmoc-Ser(*t*-Bu)−OH, PYBOP, N,*N*′-diisopropylcarbodiimide (DIC), N,N-diisopropylamine (DIEA), DMF, 25 °C, 4 h. (c) 20% piperidine/DMF, 25 °C, 6 + 8 min. (d) Fmoc-Xaa−OH, 1-hydroxybenzotriazole (HOBt), N,*N*′-diisopropylcarbodiimide (DIC), DMF, 25 °C, 2 h. (e) Trifluoroacetic acid (TFA)/triisopropylsilane (TIS)/H2O = 95:2.5:2.5 (v/v/v), 0 → 25 °C, 2 h.

mitochondria. Meanwhile, the N-terminal part of the Desmin molecule might encompass targeting signals that are capable of localizing the protein to the outer mitochondrial membrane (OMM). The peptide **T6-S** is precisely situated in the N-terminal portion of the Desmin molecule, which is the targeting region for the mitochondrial outer membrane. To explore whether **T6-S** possesses the ability to target the mitochondrial outer membrane and enhance mitochondrial function, we attached a FITC fluorescent group to the N-terminal end of **T6-S** via genetic engineering. The outcomes of the fluorescence confocal microscopy experiment indicated that **T6-S** was colocalized with the mitochondrial outer membrane, thereby validating our hypothesis (Figure 2G).

Modification and Evaluation of Peptides. Based on the screening of the active site of the mother peptide and the conformational analysis of **T6-S**, Fmoc protection strategy was employed to design and synthesize a multitude of valuable peptides via solid-phase approaches (Figure 3A). As shown in Scheme 1, Wang resin **A1** was modified with Fmoc-Ser(*t*-Bu)−OH, PYBOP, and the coupling agent HOBT under alkaline conditions for the solid-phase coupling reaction, thereby obtaining **A2**. 20% piperidine was utilized to eliminate the Fmoc group, leading to **A3**. Subsequently, **A3** underwent repeated steps of deprotection and coupling reactions in a "from-end-to-beginning" fashion to acquire the free intermediate **A4**, followed by cleavage to remove all protective groups, generating the final crude product **T6-S**. Afterward, the product was further refined by preparative reverse-phase high-performance liquid chromatography (RP-HPLC) and characterized by analytical high-performance liquid chromatography (HPLC) and electrospray ionization mass spectrometry (ESI-MS). According to this strategy, the modified peptides apart from C-short amide and the ring peptide **S19** can be attained.

First, cell growth was assessed with treatment of **T6-S** at various concentrations by the CCK-8 assay, where we observed that even at a high concentration (64.0 μM), **T6-S** did not affect the growth of LX2 cells (Figure S1E,F). Next, the inhibitory effects exerted by the aforementioned peptide on the expression of FN and COL1α1 in LX2 cells were investigated. The outcomes of the protein blot analysis (Figure 3B−E), affirm that we introduced three non-natural amino acids, namely 2-methylalanine (Aib), 2-ethylalanine (Iva), and norvaline (Nva), at the sites of Gly^4, Ala^5, or Pro^6 to further fortify its pharmacological properties and binding affinity. It is well-known that these two amino acids can potentiate the peptide's protease resistance and augment its activity.[37,38] Moreover, it is gratifying to discover that **S17**, in which Gly^4 is substituted by Iva and Pro6 is replaced by Nva, demonstrates higher inhibitory activity than **T6-S** (Figure 3D,E). However, replacing Ala^5 with Aib, Gly^4 with Nva and Iva, and Pro^6 with Aib and Nva no longer exert inhibitory effects on FN and COL1α1 (Figure 3B,D).

Intriguingly, the inhibitory activity of peptides **S4** and **S6**, in which the fourth Gly is replaced by the acidic amino acid Asp and the basic amino acid Lys, respectively, is higher than that of

https://doi.org/10.1021/acsomega.4c10956
ACS Omega 2025, 10, 9661−9674

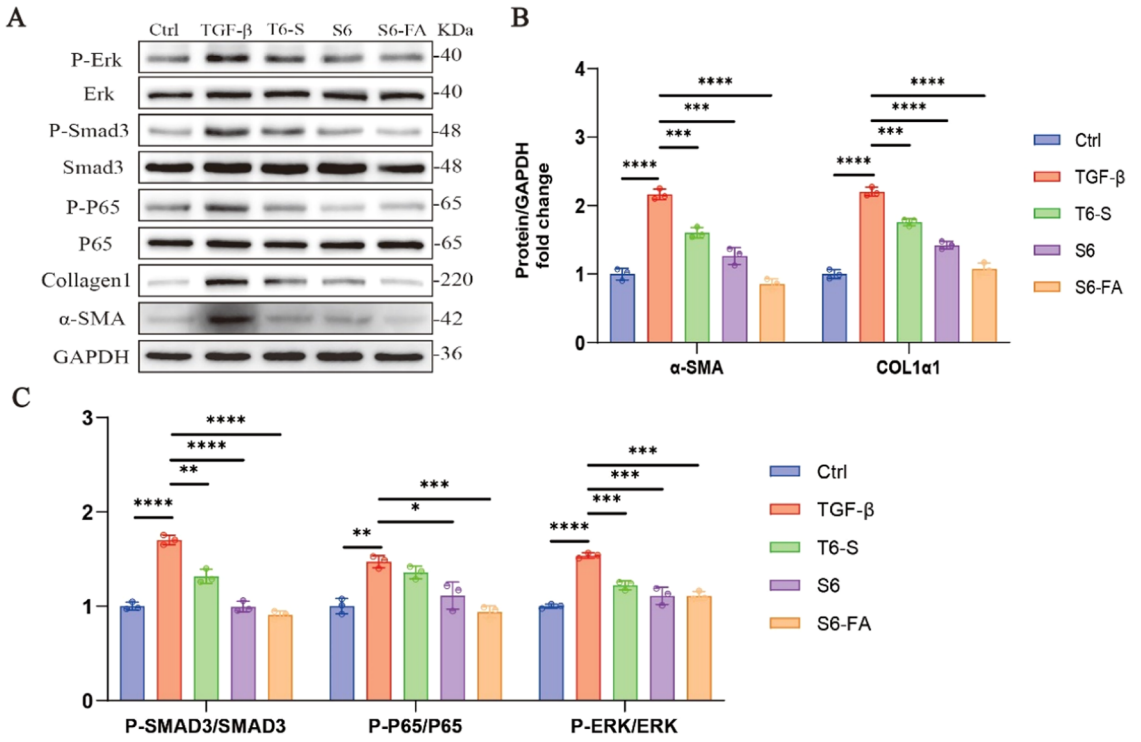

Figure 4. Validate the fibrosis pathway and its effects on phenotypic proteins in vitro. (A) Western blot analysis of p-ERK, p-Smad3, p-P65, α-SMA and COL1α1 in LX2 cells. Cells were treated with TGF-β or candidate peptides (10 μM) for 24 h. GAPDH was used as a loading control. (B) Densitometric analysis of the ERK, Smad3, and P65 phosphorylation in (A) (n = 3). (C) Densitometric analysis of the α-SMA, and COL1α1 in (A) (n = 3). Data are represented as mean ± SEM *P < 0.05, **P < 0.01, ***P < 0.001 and ****P < 0.0001.

T6-S, which indicates that altering the acidic or basic properties of the amino acids can enhance the inhibitory activity (Figure 3B,C). Moreover, the inhibitory activity of peptide **S5**, where the sixth Pro is substituted with the acidic amino acid aspartate, is higher than that of **T6-S**, whereas the inhibitory activity of peptide **S7**, in which the sixth Pro is replaced by the basic amino acid lysine, is lower (Figure 3B,C). Meanwhile, other peptides which were substituted with neutral amino acids that were less readily identifiable by enzymes did not exhibit a notable increase in inhibitory activity, which suggests that neutral amino acids such as Ser, Thr, and Leu cannot boost the inhibitory activity of the peptide (Figure 3B,C). It is notable that the C-terminal carbamylated peptide **S18** displays excellent inhibitory activity. Nevertheless, the ring peptide **S19** acquired through head-to-tail cyclization diminished the inhibitory impacts on the expression of FN and COL1α1, which might be attributed to alterations in structural conformation or flexibility (Figure 3E).

In summary, peptides **S4**, **S5**, **S6**, **S17**, and **S18** were capable of reducing the expression levels of FN and COL1α1 in LX2 cells by approximately 20−40% (Figure 3E). Among these, the peptide **S6**, in which Lys substitutes for Gly[4], was the most efficacious, with its inhibitory activity against FN and COL1α1 being approximately 1.5 times that of **T6-S**. Additionally, a dose−response analysis demonstrated that the active peptide **S6** decreased the expression of FN and COL1α1 in a dose-dependent fashion. Given that the C-terminal carboxylated **S18** displayed favorable inhibitory activity, and with the aim of optimizing the pharmacological effects and prolonging the half-life of the candidate peptides, we endeavored to design and synthesize the C-terminal carboxylated fatty acid side chain peptide **S6-FA**. To elucidate the structure−activity relationship, we conducted circular dichroism (CD) spectroscopy on four candidate peptides (**T6-S**, **S5**, **S6**, and **S6-FA**) in a 50% trifluoroethanol (TFE) aqueous solution. As illustrated in Figure 3G, **T6-S**, **S5**, and **S6** displayed characteristic absorption peaks at 208 and 222 nm, indicative of α-helical structures under these conditions. Conversely, **S6-FA** exhibited a weak negative band at 195 nm and a pronounced negative peak around 222 nm, suggesting the coexistence of both α-helical and β-turn conformations. Based on these outcomes, **S6**, **S6-FA**, and **T6-S** were chosen as potential antifibrotic candidate peptides for further in vitro and in vivo tests.

The Candidate Peptide Inhibit ERK and Smad3 Phosphorylation in vitro and Improve Inflammation in Liver Fibrosis. Hepatic fibrosis is a pathological repair process following long-term chronic liver injury, mainly through the activation of hepatic stellate cells (HSCs) and the excessive accumulation of ECM.[3,29] The activation of HSCs involves multiple genes and factors, among which the MAPK/ERK signaling pathway promotes the occurrence of hepatic fibrosis by inducing the proliferation and activation of HSCs.[5,6] Phosphorylated ERK enters the nucleus and regulates the expression of transcription factors and cyclins D and E, promoting the transition of HSCs from G1 to S phase.[4] TGF-β1 plays a key role in this process, promoting the activation and proliferation of HSCs, while inhibiting the proliferation of hepatocytes and inducing the generation and deposition of ECM, especially COL1α1. The TGF-β signaling pathway and oxidative stress jointly regulate the production of COL1α1.[8,16]

We subjected LX2 cells to treatment with **S6**, **S6-FA**, and **T6-S** to assess the effects of these peptides in modulating the expression of liver fibrosis-related markers. The experimental outcomes indicated that **S6** and **S6-FA** conspicuously decreased the expression of α-SMA and COL1α1, which are crucial

https://doi.org/10.1021/acsomega.4c10956
ACS Omega 2025, 10, 9661−9674

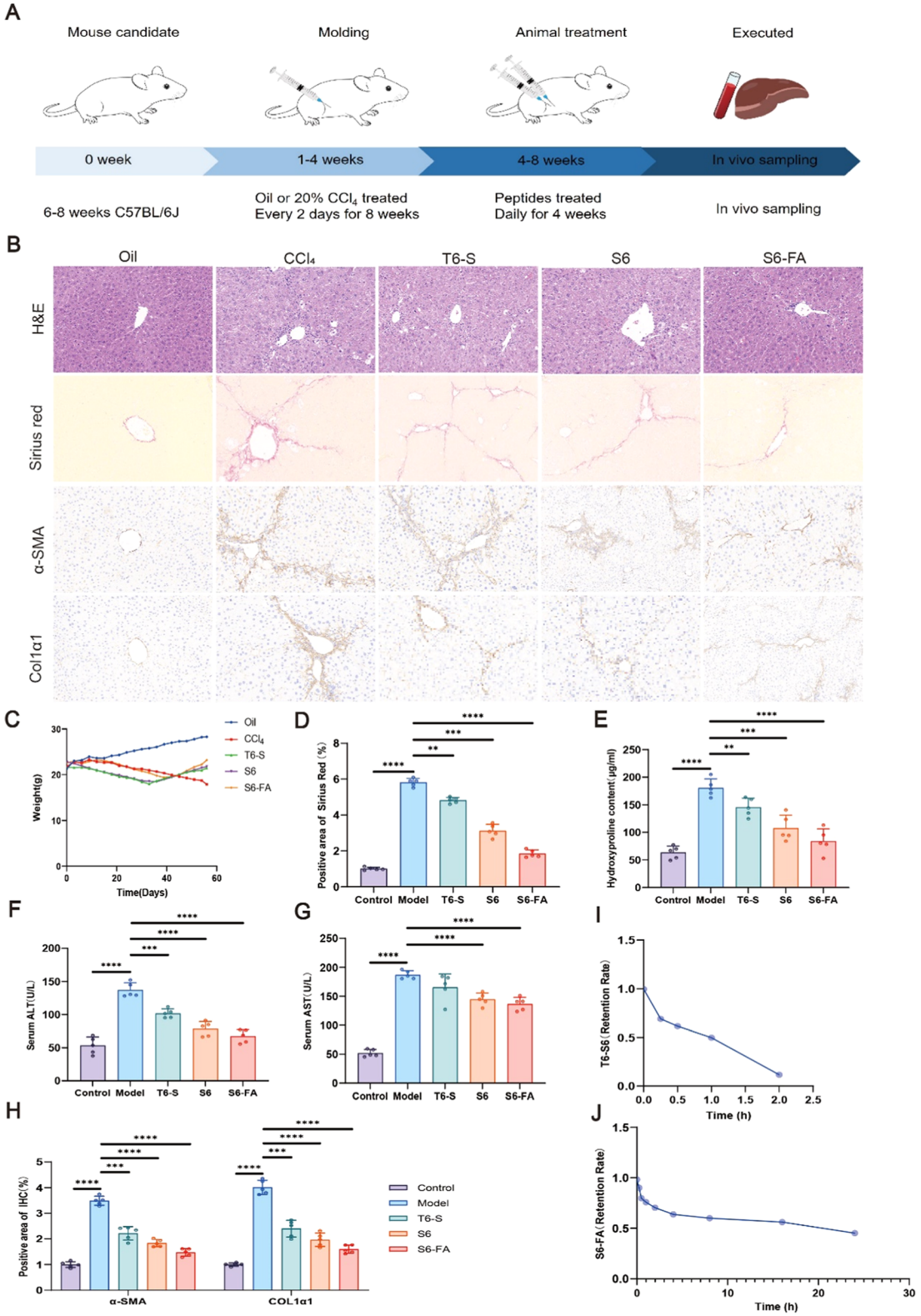

Figure 5. In vivo study of candidate peptides in a CCl_4-induced liver fibrosis model. (A) Schematic illustration of the CCl_4-indcued liver fibrosis model and the in vivo treatment procedure. (B) Histological images of hepatic tissues by H&E, Sirius red staining and immunohistochemical (IHC) staining for α-SMA, COL1α1 (magnification: 20 ×; n = 5). (C) Monitoring of changes in mouse body weight (n = 5−7). (D) Positive staining area analyses of the histological images shown in (B). (E) Analyses of hydroxyproline in liver tissue (n = 5). (F, J) Analyses of ALT and AST in serum (n = 5). (H) Analysis of Positive Staining Areas in Histological Images by Immunohistochemistry shown in (B). (I, J) The serum stability of maternal peptide T6-S and S6-FA. Data are represented as mean ± SEM $^{**}P < 0.01$, $^{***}P < 0.001$ and $^{****}P < 0.0001$.

biomarkers for HSC activation and ECM generation (Figure 4A,B). Simultaneously, these two peptides effectively suppressed the phosphorylation levels of ERK and Smad3, suggesting that they might exert their functions by interfering

https://doi.org/10.1021/acsomega.4c10956
ACS Omega 2025, 10, 9661−9674

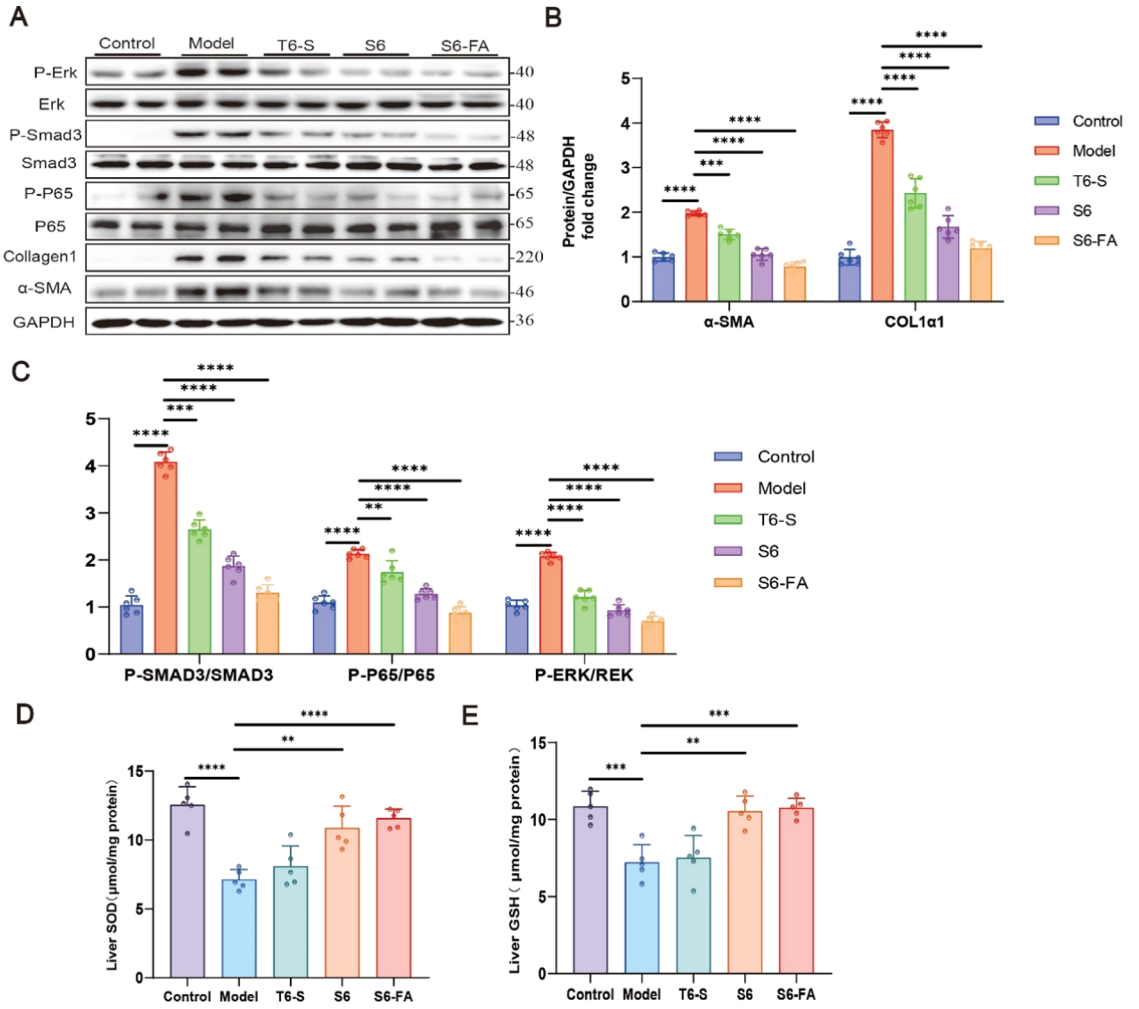

Figure 6. Validate the fibrosis pathway and its impact on phenotypic proteins, and improve oxidative stress in vivo. (A) Western blot analysis of p-ERK, p-Smad3, p-P65, α-SMA and COL1α1 in Histological tissue of the liver. (B) Densitometric analysis of the ERK, Smad3, and P65 phosphorylation in (A) (n = 5). (C) Densitometric analysis of the α-SMA, and COL1α1 in (A) (n = 5). (DE) The level of SOD and GSH based on enzyme activity assay (n = 5). Data are represented as mean ± SEM $^{**}P < 0.01$, $^{***}P < 0.001$ and $^{****}P < 0.0001$.

with the MAPK and TGF-β/Smad3 signaling pathways (Figure 4A,C). These results demonstrate that **S6** and **S6-FA** can efficaciously inhibit the activation of HSCs in LX2 cells, ameliorate liver fibrosis-related inflammatory responses, encompassing the reduction of the release of pro-inflammatory factors.

As anticipated, we further discovered that peptide **S6-FA** displayed a more salient advantage in enhancing liver fibrosis induced by LX2 cells under TGF-β stimulation. Specifically, **S6-FA** not only exhibited superiority to other treatment groups in reducing the expression of α-SMA and COL1α1 but also significantly augmented the inhibitory effect on ERK phosphorylation, thereby more effectively impeding HSCs from transforming into fibroblast-like phenotypes. These findings furnish significant evidence for comprehending the potential of this class of peptides in the treatment of liver fibrosis and lay a foundation for the development of novel antifibrotic drugs in the future.

In vivo Evaluation of Serum Stability and Liver Fibrosis of Candidate Peptides. Inspired by the in vitro findings, we utilized a CCl_4-induced liver fibrosis model to assess the impacts of **S6**, **S6-FA**, and **T6-S** on extracellular matrix (ECM) accumulation. Throughout the peptide treatment, mice that were treated with or without **S6** or **S6-FA** displayed no abnormalities in terms of appearance (encompassing hair color and luster), behavior, food intake, or body weight. Peptides were intraperitoneally administered at a dosage of 250 μg/kg daily for 4 weeks (Figure 5A,C). Additionally, compared with the control group, the liver tissue in the CCl_4 model group was harder, with varying degrees of inflammation, consolidation, and fibrosis in the liver lobules. However, the liver conditions in the S6 group (CCl_4+S6) and the S6-FA group (CCl_4+S6-FA) were improved (Figure S1A,B). The therapeutic effects showed that both S6 and S6-FA could reverse the negative effects of CCl_4 on body weight and pulmonary indicators. H&E staining and Sirius staining were carried out on liver sections to evaluate the levels of fibrosis biomarkers (Figure 5B). As shown in the Figure 5B, a significant augmentation in inflammatory infiltration and collagen deposition was observed in the CCl_4 group in contrast to the control group. **S6** and **S6-FA** demonstrated more efficacious outcomes in reducing collagen deposition compared to **T6-S** (Figure 5D). Further analysis of serum hydroxyproline (HYP) indicated that **S6** and **S6-FA** significantly decreased the HYP content in liver tissue, suggesting that **S6** and **S6-FA** can mitigate collagen deposition (Figure 5E). Moreover, mice recovering from liver dysfunction were verified to have lower serum levels of ALT and AST (Figure 5F,G). Ultimately, the

https://doi.org/10.1021/acsomega.4c10956
ACS Omega 2025, 10, 9661−9674

fibrosis markers α-SMA and COL1α1 were notably lower in the **S6** and **S6-FA** treatment groups in comparison with the control group and the **T6-S** group (Figure 5H). In conclusion, we have verified that peptides **S6** and **S6-FA** can markedly alleviate liver fibrosis induced by CCl_4.

The serum stability of peptides pertains to their capacity to preserve their structure and biological activity within serum or plasma over a definite period, which holds substantial significance in drug development and biomarker research since the stability of peptides directly influences in vivo bioavailability, metabolism, and clearance.[39] Experimental approaches such as incubating peptides in serum and monitoring concentration alterations are crucial for evaluating peptide stability both in vitro and in vivo.[40] Despite the fact that peptides **S6**, **S6-FA**, and **T6-S** display outstanding antifibrotic effects in vitro, it is of paramount importance to elucidate their serum stability in vivo. Hence, we evaluated the stability of peptides **T6-S** and **S6-FA** in mouse serum. As presented in the table, merely 61% and 50% of **T6-S** were detectable by HPLC after incubation in serum for 30 min and 1 h respectively, and only 12% were detectable after 2 h of incubation, suggesting nearly complete degradation and clearance (Figure 5I). To our gratification, **S6-FA** manifested significantly superior serum stability, with a half-life approximating 24 h (Figure 5J). Based on these outcomes, augmenting the fatty acid side chain of peptides might prevent rapid clearance in vivo, and peptide **S6-FA** possesses more beneficial serum stability characteristics compared to **T6-S**.

To confirm whether **S6** and **S6-FA** can inhibit the phosphorylation of ERK and Smad3, decrease ECM protein synthesis, and ameliorate liver fibrosis inflammation in vivo, thereby alleviating liver fibrosis in CCl_4 mice, we carried out Western blot experiments for verification. As anticipated, **S6** and **S6-FA** effectively inhibited the phosphorylation of ERK and Smad3 (Figure 6A,C), and reduced the synthesis of the majority of α-smooth muscle actin (α-SMA) and COL1α1 (Figure 6A,B). Moreover, the fatty acid side chain peptide **S6-FA** was capable of improving CCl_4-induced liver fibrosis at low doses, demonstrating superior therapeutic effects compared to peptide **S6**. In summary, these discoveries indicate that the fatty acid side chain peptide **S6-FA** can effectively obstruct the relevant pathways of liver fibrosis development and improvement in the CCl_4 model, and effectively enhance liver fibrosis, revealing its potential for the treatment of liver fibrosis.

Peptide Reduces Oxidative Stress and Improves Mitochondrial Function. Currently, some studies have specifically designed peptides to target mitochondria, aiming to enhance their antioxidative and antiaging effects and optimize mitochondrial function.[41,42] Previous studies have shown that our peptides possess the ability to target the mitochondrial membrane, but have not yet been examined in terms of improving mitochondrial function. In this study, we explored whether the candidate peptides have the potential to improve mitochondrial oxidative stress, particularly in regulating the redox balance at the tissue level. Superoxide dismutase (SOD) and glutathione (GSH) are significant antioxidants within the body. Their main function is to eliminate superoxide anions and other oxygen free radicals in cells, protecting cells from oxidative stress damage and playing a crucial role in detoxification and antioxidation.[43] Oxidative stress is triggered by excessive reactive oxygen species (ROS) in the body, among which superoxide anions are the most common type. SOD reduces the accumulation of ROS by converting superoxide anions into hydrogen peroxide (H_2O_2) and oxygen, thereby protecting cells from oxidative damage.[44,45] As depicted in the figure, we discovered that the contents of SOD and GSH in the liver tissue of the peptide **S6** and **S6-FA** treatment groups were significantly higher than those of the CCl_4 group (Figure 6D,E). This finding suggests that these peptides have the potential to alleviate oxidative stress.

These results indicate that peptides **S6** and **S6-FA** can effectively reduce oxidative stress caused by CCl_4-induced liver fibrosis and improve cellular environment by regulating mitochondrial function. It is worth noting that peptide **S6-FA** showed better improvement effects compared to **T6-S** in this study. Under CCl_4 induction, mitochondrial dysfunction leads to insufficient energy generation and the production of more harmful substances such as ROS, which further aggravates liver injury. Therefore, by targeting mitochondria and enhancing their antioxidant capacity, these candidate peptides may provide new strategies for treating age-related or chronic diseases triggered by environmental factors.

DISCUSSION

Liver fibrosis is a process in which normal liver tissue is gradually replaced by fibrous connective tissue in the long-term chronic injury of the liver.[1,2] It is usually an important pathological process in chronic liver diseases (such as chronic viral hepatitis, alcoholic liver disease, and nonalcoholic fatty liver disease, etc.) and is driven by the excessive accumulation of ECM proteins in the extracellular matrix.[5,6] It is the key factor in the hardening of the liver. Long-term liver injury leads to continuous liver cell necrosis and inflammatory responses, activating hepatic stellate cells to transform into fibroblasts, starting to overproduce and secrete collagen, fibronectin, and laminin, etc. These ECM proteins accumulate in the liver and form fibrotic connective tissue, gradually replacing the normal liver structure, leading to liver dysfunction. If it is not diagnosed and treated in time, liver fibrosis may progress to cirrhosis, even leading to liver failure and liver cancer.[1,7,9] Employing peptide 6 (T6), an endogenous peptide present in the adhesive tissue of uterine fibrosis, our aim was to inhibit the fibrosis induced by TGF-β1 in human myometrial stromal cell lines and primary human myometrial stromal cells.[9] TGF-β brings about liver fibrosis by activating hepatic stellate cells (HSCs) and facilitating fibrosis, thereby propelling the advancement of fibrotic diseases.[46] Hence, our intention was to explore whether T6 has functional impacts on liver fibrosis.

We initially performed an alanine scan on T6 to assess the specific amino acid residues that exert a crucial role in the antifibrotic activity. Our investigation results demonstrated that residues Gly^4, Phe^6, Leu^{14}, Ser^{16}, Pro^{19}, and Arg^{20} exerted negligible influence on the inhibitory activity of the parent peptide against FN and COL1α1 and might be appropriate for further structural optimization to enhance the biological activity. In contrast, residues The1, Phe^2, Gly^7-Phe^8-Pro^9-Leu^{10} were of paramount importance for their inhibitory activity against FN and COL1α1. Consequently, we carried out a C-terminal truncation until the peptide lost its antiliver fibrotic activity at the Pro^9 residue, thereby affirming the significance of these residues in the peptide's antiliver fibrotic activity.

Based on the screening of the active site of the mother peptide and the conformational analysis of **T6-S**, we designed and synthesized a series of modified peptides. According to the above results, **S17** with Gly^4 replaced by Iva and Pro^6 replaced by Nva exhibits higher inhibitory activity than **T6-S**, while the

https://doi.org/10.1021/acsomega.4c10956
ACS Omega 2025, 10, 9661−9674

peptides with Aib replacing Ala[5], Nva replacing Gly[4], and Iva replacing Pro[6] lose their inhibitory effects on FN and COL1α1. Surprisingly, changing the acidity of amino acids can enhance the inhibitory activity, for example, the peptides **S4**, **S6** with Gly[4] replaced by Asp and Lys, and **S5** with Pro[6] replaced by Asp, all have higher inhibitory activity than **T6-S**. In addition, peptides with neutral and less space-occupying amino acids have not significantly improved the inhibitory activity. It is worth noting that the C-terminal carboxylated **S18** also exhibits good inhibitory activity, but the cyclic peptide **S19** reduces the inhibitory effect on the expression of FN and COL1α1.

Linear peptides exhibit suboptimal targeting in vivo, potentially causing the drug to act upon nontarget tissues and augment side effects; they are prone to enzymatic degradation, resulting in a shortened biological half-life and exerting an adverse impact on the drug's efficacy; the release of the peptide within the body might be insufficiently controllable, giving rise to fluctuations in drug concentration and influencing the therapeutic outcome; and they may not be entirely compatible with the body's internal environment, leading to immune responses or toxic issues.[12,19] Hence, it is of utmost urgency to enhance the efficacy of the drug while minimizing the risk of adverse reactions. Numerous studies have demonstrated that the incorporation of fatty acid side chains into peptides typically exhibits excellent biocompatibility and biodegradability, reducing toxicity to the organism.[19,20] Owing to its distinctive structure, this type of peptide can attain targeted therapy by modulating its binding to specific receptors, enhancing the efficacy of the drug and reducing side effects, and is well-suited for drug delivery systems. Based on this, we designed and synthesized the C-terminal amide-modified fatty acid side chain peptide **S6-FA**. We chose **S6** and **S6-FA** for in vivo pharmacological efficacy verification in mice induced by CCl_4 because they possess the most optimal inhibitory activity against liver fibrosis biomarkers such as FN, α-SMA, and COL1α1 in vitro. Unfortunately, although we conducted molecular dynamics simulations to refine the relationship between peptide **T6-S** and its target, the absence of the **T6-S** target precluded us from further delving into the interaction between the peptide ligand and the target protein, which requires further optimization in the design of therapeutic peptides and clarification of the mechanistic pathways for the treatment of liver fibrosis.

The data from in vitro and in vivo candidate peptide treatment for fibrosis show that peptides **S6** and **S6-FA** significantly reduced the expression of α-SMA and COL1α1 in LX2 cells, effectively inhibited the phosphorylation of ERK and Smad3, and improved inflammation in liver fibrosis. Furthermore, in the liver tissue of the CCl4-induced model, peptide S6 and S6-FA can significantly increase the content of SOD and GSH, and reduce the level of ROS. Notably, Due to the fact that the fatty acid side chains can effectively enhance the stability of peptides in serum by improving the hydrophobicity of polypeptides, strengthening the binding with carrier proteins, increasing resistance to enzymatic hydrolysis, regulating conformational stability, and reducing immune clearance. In this study, it was observed that the fatty acid side chain peptide **S6-FA** showed better improvement effects compared to **T6-S**, which could disrupt the relevant pathways of liver fibrosis development and effectively improve liver fibrosis, indicating its potential for treatment of liver fibrosis. This suggests that when conducting further in-depth research in the future, we may consider exploring the influence of different structural features on their biological activity to optimize these peptides as potential therapeutic agents for clinical use.

CONCLUSIONS

In summary, we obtained the novel peptide **S6-FA** which had higher antiliver fibrosis activity and a longer half-life through the structure−activity relationship studies and rational modification of T6. The research indicated that **S6-FA** was capable of suppressing the activation of hepatic stellate cells and diminishing the secretion of COL1α1 and FN. Additionally, it alleviated liver fibrosis by regulating the Erk, Smad, and P65 pathways. Further animal studies demonstrated that **S6-FA** decreased COL1α1 and α-SMA expression induced by CCl_4 in mouse models, enhanced liver fibrosis and inflammatory responses. Moreover, it has been discovered that **S6-FA** can enhance the contents of SOD and GSH in tissues and decrease the generation of ROS, thereby mitigating the oxidative stress induced by CCl_4. In summary, this study explored the structure and conformation of peptide **T6-S** and further optimized its structure to develop a novel long-acting peptide **S6-FA**, with enhanced antifibrotic activity both in vitro and in vivo. This study presents a highly effective and promising drug strategy targeting mitochondria and a new candidate compound for antifibrotic therapy.

MATERIALS AND METHODS

Materials and Instruments for Chemistry. All solvents, all standard Fmoc-protected amino acids, Rink amide 4-methylbenzhy-drylamine (MBHA) resin, and 2-chorotrityl chloride (2-CTC) resin were used directly as received from commercial suppliers. Solid-phase peptide synthesis (SPPS) was performed manually on a chemical rotary vibrator. The purification of the final compounds was carried out on a Thermo Fisher Ultimate 3000 HPLC system, with the column: Thermo Fisher C18 column (5 μm, 20 mm × 250 mm). The mass spectra (MS) were recorded on the Agilent 1260−6120 HPLC-MS, Thermo Fisher LTQ-XL UPLC-MS, or Waters ZQ 2000 HPLC-MS mass spectrometer (ionization method: electrospray ionization (ESI)). The purity of the final compounds was determined by the Agilent 1260 HPLC system or the Thermo Fisher Ultimate 3000 HPLC system, with the column: Thermo Fisher C18 250 × 4.6 mm2 5 μ−100A. It was found that the purity of all final compounds was greater than 95%.

Cell Model. Human hepatic stellate cell line LX2 was purchased from Type Culture Collection of Chinese Academy of Sciences (Shanghai, China). Cells were cultured in Dulbecco's modified Eagle's medium (DMEM) containing 10% fetal bovine serum (FBS) and 1% penicillin-streptomycin (Thermo Fisher Scientific) at 37 °C in a 5% CO_2 humidified atmosphere. LX2 cells were incubated with TGF-β in the absence or presence of 10 μM peptides for 24 h.

Molecular Dynamic Simulations. The Amber16 program package was employed for equilibrium molecular dynamics simulations. The FF14SB force field and the Gaff force field were utilized to depict the structure of each standard/nonstandard residue in the polypeptide molecule, and the Amber16 program was adopted to conduct a 50 ns NVT ensemble for each polypeptide molecular structure in an explicit solvent environment (T = 300 K) molecular dynamics simulation. Prior to the simulation, the steepest descent method and the conjugate gradient method were utilized to optimize the geometric

https://doi.org/10.1021/acsomega.4c10956
ACS Omega 2025, 10, 9661−9674

structure of the composite system and then the composite system was gradually heated from 0 to 300 K. A temperature coupling algorithm was utilized to control the temperature of the system at 300 K. During the simulation, the PME method was employed to calculate the long-range electrostatic interactions, and the SHAKE algorithm was adopted to handle hydrogen-related stretching vibrations. The cutoff value of the long-range interactions was set at 10 Å, and the simulation step size was 2 fs. After the simulation was accomplished, the Cpptraj program was utilized to extract the requisite information from the MD trajectory and undertake energy analysis and trajectory analysis, including root-mean-square shift (RMSD), root-mean-square fluctuation (RMSF), hydrogen bond analysis, and structural cluster analysis of the entire trajectory.

Western Blot Analysis. Total protein was extracted from cell or liver samples using RIPA lysis buffer (Beyotime Biotechnology, Shanghai, China) and quantified with the BCA assay kit (Pierce, Thermo Fisher Scientific). The proteins were separated by SDS-PAGE based on the target protein size and subsequently transferred to a pre-equilibrated poly(vinylidene difluoride) membrane (PVDF, Immobilon-PSQ transfer membranes, Merck Millipore, Germany). The membranes were incubated overnight at 4 °C with primary antibodies. Following incubation with secondary antibodies, proteins were visualized using enhanced chemiluminescence (GlarityTM Western ECL Substrate, Bio-Rad), and the resulting signals were captured and analyzed using Tanon-Image Software (Shanghai, China). GAPDH was employed as a reference antibody for data normalization. Details regarding the antibodies can be found in Supporting Information Tables S5−S9. All compounds utilized had a purity greater than 95% as determined by HPLC analysis.

Animal Models and Tissue Collection. The mice utilized in this research were healthy and exhibited normal immune function, maintained in a specific-pathogen-free environment with a 12 h light-dark cycle. They had unrestricted access to food and water. All animal research protocols complied with the U.S. Public Health Service Policy regarding laboratory animals and received approval from the Ethics Committee for Animal Use and Care at Sun Yat-sen University.

Male C57BL/6J mice, aged between 6 to 8 weeks and weighing between 20 to 24 g, were sourced from the Guangdong Medical Experimental Animal Center. They were housed in cages maintained at a temperature range of 20−25 °C with a light/dark cycle of 12 h each for a duration of 12 h. Mice had unrestricted access to food and water. Following the final drug administration, the mice underwent a fasting period of 9 h before being euthanized after an additional interval of 8 h. The liver tissues were quickly frozen using liquid nitrogen and subsequently stored at −80 °C for later analysis or fixed in a solution of 10% formaldehyde for histological examination. Blood samples were collected via retro-orbital venipuncture from anesthetized subjects, followed by centrifugation at a force of 1000g for 15 min to separate serum, which was then preserved at −80 °C for future assessments.

Mice were induced to develop liver fibrosis by subcutaneous injection of 20% CCl_4 (Sigma, China) in corn oil (Aladdin, China) every 2 days for 8 weeks (5 mL/kg body weight). Mice injected with an equal volume of corn oil served as controls. The last 4 weeks of the treatment were used to evaluate the pharmacological effects in mice with liver fibrosis (250 μg/kg; intraperitoneal injection daily). The purity of all compounds used was >95%, as determined by HPLC analysis. For each group, $n = 5$.

Serum and Tissue Biochemical Assays. The concentrations of alanine aminotransferase (ALT) and aspartate aminotransferase (AST) in serum were measured using specific commercial assay kits from Nanjing Jiancheng Bioengineering Institute, China. All compounds utilized had a purity greater than 95% as confirmed by HPLC analysis. For each group, $n = 5$.

Determination of Hydroxyproline Content. Approximately 10 mg of liver tissue was collected from each mouse, and the level of hydroxyproline (HYP) was quantified, as HYP is an indicator of the in vivo degradation of collagen. For this purpose, the HYP assay kit from Nanjing (produced by the Jiancheng Bioengineering Institute in Nanjing, China) was used, and the experiment was conducted according to the manufacturer's instructions. For each group, $n = 5$.

Organ Histopathological Assessment. The liver was embedded in paraffin, and liver slices were fabricated. After deparaffinization and rehydration, the sections were stained with hematoxylin and eosin (H&E). For the Sirius red analysis, 10 photographs of the low-magnification field (20×) were captured for each liver sample. Immunohistochemical (IHC) staining was performed according to the manufacturer's instructions. Quantitative analysis of positive staining areas was performed on all liver sections using the open-source software (ImageJ software (http://imagej.nib.gov/)). Large bile ducts and vessels were excluded. For each group, $n = 5$.

Serum Stability Analysis. Five mM peptides were incubated with mouse serum for 0, 0.25, 1, 2, 4, 8, 16, and 24 h at 37 °C. Subsequently, ice-cold acetonitrile was added to quench the reaction, followed by vortex mixing for 10 s. The mixture was then allowed to stand for 1 min. Deionized water containing 1% trifluoroacetic acid (TFA) was subsequently added to ensure complete termination of the reaction. Then, mixtures were centrifuged (13,000*g*, 10 min) to obtain the supernatant. Reverse-phase high-performance liquid chromatography−mass spectrometry (RP-HPLC-MS) was employed to analyze the content of candidate peptides. The serum stability of candidate peptides was presented as the retention rate of each peptide. Mobile phase: A: 0.1% TFA; B: acetonitrile, with gradient elution of B: 5−95%; 30 min.

Quantification and Statistical Analysis. The positive area of stained tissue slices was quantified using ImageJ software (https://imagej.nih.gov/ij/). Statistical analysis was performed using GraphPadPrism 9.0 (https://www.graphpad.com/), and all data are presented as mean ± SD (standard deviation). Differences were compared using Student's t test, and $p < 0.05$ was considered statistically significant.

■ ASSOCIATED CONTENT

Supporting Information

The Supporting Information is available free of charge at https://pubs.acs.org/doi/10.1021/acsomega.4c10956.

The original Western blot images, raw data, animal experiment-related data, as well as the steps for polypeptide synthesis and characterization images (PDF)

■ AUTHOR INFORMATION

Corresponding Authors

Xianxing Jiang − *State Key Laboratory of Anti-Infective Drug Discovery and Development, School of Pharmaceutical*

https://doi.org/10.1021/acsomega.4c10956
ACS Omega 2025, 10, 9661−9674

Sciences, Sun Yat-sen University, Guangzhou, Guangdong 510006, China; orcid.org/0000-0002-7508-2368; Email: jiangxx5@mail.sysu.edu.cn

Yifeng Zhou − *College of Life Science, China Jiliang University, Hangzhou, Zhejiang 310018, China;* orcid.org/0000-0002-0453-7230; Email: zhouyifeng@cjlu.edu.cn

Wanxiang Jiang − *Sichuan Greentech Bioscience Co., Ltd, Meishan, Sichuan 620031, China*; Email: jiang.wx@greentech-bio.com

Authors

Mingmin Li − *College of Life Science, China Jiliang University, Hangzhou, Zhejiang 310018, China*

Liang Qi − *State Key Laboratory of Anti-Infective Drug Discovery and Development, School of Pharmaceutical Sciences, Sun Yat-sen University, Guangzhou, Guangdong 510006, China*

Jin Huang − *Guangzhou Dorsay Biotechnology Co., Ltd, Guangzhou, Guangdong 510006, China*

Haonan Li − *State Key Laboratory of Anti-Infective Drug Discovery and Development, School of Pharmaceutical Sciences, Sun Yat-sen University, Guangzhou, Guangdong 510006, China*

Wei Cheng − *State Key Laboratory of Anti-Infective Drug Discovery and Development, School of Pharmaceutical Sciences, Sun Yat-sen University, Guangzhou, Guangdong 510006, China*

Zihan Shi − *State Key Laboratory of Anti-Infective Drug Discovery and Development, School of Pharmaceutical Sciences, Sun Yat-sen University, Guangzhou, Guangdong 510006, China*

Complete contact information is available at: https://pubs.acs.org/10.1021/acsomega.4c10956

Author Contributions

⊥M.L., and L.Q. contributed equally to this study.

Notes

The authors declare no competing financial interest.

■ ACKNOWLEDGMENTS

This work was supported by "Noncommunicable Chronic Diseases-National Science and Technology Major Project" (No. 2023ZD0502300); the National Natural Science Foundation of China (No. 22378376); and the National Natural Science Foundation of China (No. 82273761); the Nansha Key Field Science and Technology Project (No. 2024ZD003).

■ REFERENCES

(1) Horn, P.; Tacke, F. Metabolic reprogramming in liver fibrosis. *Cell Metab.* **2024**, *36* (7), 1439−1455.

(2) Yan, Z.; Cheng, X.; Wang, T.; Hong, X.; Shao, G.; Fu, C. Therapeutic potential for targeting Annexin A1 in fibrotic diseases. *Genes Dis.* **2022**, *9* (6), 1493−1505.

(3) Parola, M.; Pinzani, M. Liver fibrosis: Pathophysiology, pathogenetic targets and clinical issues. *Mol. Aspects Med.* **2019**, *65*, 37−55.

(4) Pellicoro, A.; Ramachandran, P.; Iredale, J. P.; Fallowfield, J. A. Liver fibrosis and repair: immune regulation of wound healing in a solid organ. *Nat. Rev. Immunol.* **2014**, *14* (3), 181−194.

(5) Xu, H.; Zhao, Q.; Song, N.; Yan, Z.; Lin, R.; Wu, S.; Jiang, L.; Hong, S.; Xie, J.; Zhou, H.; Wang, R.; Jiang, X. AdipoR1/AdipoR2 dual agonist recovers nonalcoholic steatohepatitis and related fibrosis via endoplasmic reticulum-mitochondria axis. *Nat. Commun.* **2020**, *11* (1), No. 5807.

(6) Kisseleva, T.; Brenner, D. Molecular and cellular mechanisms of liver fibrosis and its regression. *Nat. Rev. Gastroenterol. Hepatol.* **2021**, *18* (3), 151−166.

(7) Younossi, Z.; Anstee, Q. M.; Marietti, M.; Hardy, T.; Henry, L.; Eslam, M.; George, J.; Bugianesi, E. Global burden of NAFLD and NASH: trends, predictions, risk factors and prevention. *Nat. Rev. Gastroenterol. Hepatol.* **2018**, *15* (1), 11−20.

(8) Roehlen, N.; Crouchet, E.; Baumert, T. F. Liver Fibrosis: Mechanistic Concepts and Therapeutic Perspectives. *Cells* **2020**, *9* (4), 875 DOI: 10.3390/cells9040875.

(9) Wang, C.; Bai, Y.; Li, T.; Liu, J.; Wang, Y.; Ju, S.; Yao, W.; Xiong, B. Ginkgetin exhibits antifibrotic effects by inducing hepatic stellate cell apoptosis via STAT1 activation. *Phytother Res.* **2024**, *38* (3), 1367−1380.

(10) Lazarus, J. V.; Mark, H. E.; Anstee, Q. M.; Arab, J. P.; Batterham, R. L.; Castera, L.; Cortez-Pinto, H.; Crespo, J.; Cusi, K.; Dirac, M. A.; Francque, S.; George, J.; Hagstrom, H.; Huang, T. T.; Ismail, M. H.; Kautz, A.; Sarin, S. K.; Loomba, R.; Miller, V.; Newsome, P. N.; Ninburg, M.; Ocama, P.; Ratziu, V.; Rinella, M.; Romero, D.; Romero-Gomez, M.; Schattenberg, J. M.; Tsochatzis, E. A.; Valenti, L.; Wong, V. W.; Yilmaz, Y.; Younossi, Z. M.; Zelber-Sagi, S.; Consortium, N. C.; et al. Advancing the global public health agenda for NAFLD: a consensus statement. *Nat. Rev. Gastroenterol. Hepatol.* **2022**, *19* (1), 60−78.

(11) Romier, B.; Ivaldi, C.; Sartelet, H.; Heinz, A.; Schmelzer, C. E. H.; Garnotel, R.; Guillot, A.; Jonquet, J.; Bertin, E.; Gueant, J. L.; Alberto, J. M.; Bronowicki, J. P.; Amoyel, J.; Hocine, T.; Duca, L.; Maurice, P.; Bennasroune, A.; Martiny, L.; Debelle, L.; Durlach, V.; Blaise, S. Production of Elastin-Derived Peptides Contributes to the Development of Nonalcoholic Steatohepatitis. *Diabetes* **2018**, *67* (8), 1604−1615.

(12) Klingbeil, C. G.; Gibson, C.; Johnson, N. L.; Polfuss, M.; Gralton, K.; Lerret, S. M. Nurses' Experiences Implementing e PED: An iPad Application to Guide Quality Discharge Teaching. *Comput. Inform. Nurs.* **2022**, *40* (12), 848−855.

(13) Yang, M.; Yang, Y. Logit analysis for comparison of treatment effects of categorical data. *Hua Xi Yi Ke Da Xue Xue Bao* **1987**, *18* (2), 153−156.

(14) Toupance, S.; Brassart, B.; Rabenoelina, F.; Ghoneim, C.; Vallar, L.; Polette, M.; Debelle, L.; Birembaut, P. Elastin-derived peptides increase invasive capacities of lung cancer cells by post-transcriptional regulation of MMP-2 and uPA. *Clin Exp Metastasis* **2012**, *29* (5), 511−522.

(15) Zhang, X.; Zhou, J.; Zhu, Y.; He, L.; Pang, Z.; Wang, Z.; Xu, C.; Zhang, C.; Hao, Q.; Li, W.; Zhang, W.; Zhang, Y.; Li, M. d-amino acid modification protects N-Acetyl-seryl-aspartyl-lysyl-proline from physiological hydroxylation and increases its antifibrotic effects on hepatic fibrosis. *IUBMB Life* **2019**, *71* (9), 1302−1312.

(16) Song, X.; Shi, J.; Liu, J.; Liu, Y.; Yu, Y.; Qiu, Y.; Cao, Z.; Pan, Y.; Yuan, X.; Chu, Y.; Wu, D. Recombinant truncated latency-associated peptide alleviates liver fibrosis in vitro and in vivo via inhibition of TGF-beta/Smad pathway. *Mol. Med.* **2022**, *28* (1), 80.

(17) Hua, X.; Zhang, Y.; Xu, J.; Xu, L.; Shi, Y.; Yang, D.; Gu, X.; Wang, S.; Jia, X.; Xu, F.; Chen, J.; Ying, X. Peptidome analysis of human intrauterine adhesion tissues and the identification of antifibrotic peptide. *J. Biomed Res.* **2022**, *36* (4), 280−296.

(18) Dewidar, B.; Meyer, C.; Dooley, S.; Meindl-Beinker, A. N. TGF-beta in Hepatic Stellate Cell Activation and Liver Fibrogenesis-Updated 2019. *Cells* **2019**, *8* (11), 1419 DOI: 10.3390/cells8111419.

(19) Zhang, Q. Y.; Yan, Z. B.; Meng, Y. M.; Hong, X. Y.; Shao, G.; Ma, J. J.; Cheng, X. R.; Liu, J.; Kang, J.; Fu, C. Y. Antimicrobial peptides: mechanism of action, activity and clinical potential. *Mil Med. Res.* **2021**, *8* (1), 48.

(20) Wang, L.; Wang, N.; Zhang, W.; Cheng, X.; Yan, Z.; Shao, G.; Wang, X.; Wang, R.; Fu, C. Therapeutic peptides: current applications and future directions. *Signal Transduct Target Ther.* **2022**, *7* (1), 48.

(21) Brems, D. N.; Alter, L. A.; Beckage, M. J.; Chance, R. E.; DiMarchi, R. D.; Green, L. K.; Long, H. B.; Pekar, A. H.; Shields, J. E.;

Frank, B. H. Altering the association properties of insulin by amino acid replacement. *Protein Eng., Design Selection* **1992**, *5* (6), 527−533.
(22) Lau, J.; Bloch, P.; Schaffer, L.; Pettersson, I.; Spetzler, J.; Kofoed, J.; Madsen, K.; Knudsen, L. B.; McGuire, J.; Steensgaard, D. B.; Strauss, H. M.; Gram, D. X.; Knudsen, S. M.; Nielsen, F. S.; Thygesen, P.; Reedtz-Runge, S.; Kruse, T. Discovery of the Once-Weekly Glucagon-Like Peptide-1 (GLP-1) Analogue Semaglutide. *J. Med. Chem.* **2015**, *58* (18), 7370−7380.
(23) Kharovenko, N. M. Hygienic evaluation of the instruction of students of secondary vocational-technical mining schools. *Gig. Sanit.* **1979**, No. 7, 42−43.
(24) Song, N.; Xu, H.; Liu, J.; Zhao, Q.; Chen, H.; Yan, Z.; Yang, R.; Luo, Z.; Liu, Q.; Ouyang, J.; Wu, S.; Luo, S.; Ye, S.; Lin, R.; Sun, X.; Xie, J.; Lan, T.; Wu, Z.; Wang, R.; Jiang, X. Design of a highly potent GLP-1R and GCGR dual-agonist for recovering hepatic fibrosis. *Acta Pharm. Sin B* **2022**, *12* (5), 2443−2461.
(25) Zimmermann, T.; Thomas, L.; Baader-Pagler, T.; Haebel, P.; Simon, E.; Reindl, W.; Bajrami, B.; Rist, W.; Uphues, I.; Drucker, D. J.; Klein, H.; Santhanam, R.; Hamprecht, D.; Neubauer, H.; Augustin, R. BI 456906: Discovery and preclinical pharmacology of a novel GCGR/GLP-1R dual agonist with robust anti-obesity efficacy. *Mol. Metab* **2022**, *66*, No. 101633.
(26) Shamoto, O.; Komuro, K.; Sugisawa, N.; Chen, T. H.; Nakamura, H.; Fuse, S. Peptide Cyclization by the Use of Acylammonium Species. *Angew. Chem., Int. Ed. Engl.* **2023**, *62* (27), No. e202300647.
(27) Dougherty, P. G.; Sahni, A.; Pei, D. Understanding Cell Penetration of Cyclic Peptides. *Chem. Rev.* **2019**, *119* (17), 10241−10287.
(28) Li, R.; Wang, X.; Yin, K.; Xu, Q.; Ren, S.; Wang, X.; Wang, Z.; Yi, Y. Fatty acid modification of antimicrobial peptide CGA-N9 and the combats against Candida albicans infection. *Biochem. Pharmacol.* **2023**, *211*, No. 115535.
(29) Wynn, T. A.; Ramalingam, T. R. Mechanisms of fibrosis: therapeutic translation for fibrotic disease. *Nat. Med.* **2012**, *18* (7), 1028−1040.
(30) Ng, S.; Brueckner, A. C.; Bahmanjah, S.; Deng, Q.; Johnston, J. M.; Ge, L.; Duggal, R.; Habulihaz, B.; Barlock, B.; Ha, S.; Sadruddin, A.; Yeo, C.; Strickland, C.; Peier, A.; Henry, B.; Sherer, E. C.; Partridge, A. W. Discovery and Structure-Based Design of Macrocyclic Peptides Targeting STUB1. *J. Med. Chem.* **2022**, *65*, 9789 DOI: 10.1021/acs.jmedchem.2c00406.
(31) Dutour-Provenzano, G.; Etienne-Manneville, S. Intermediate filaments. *Curr. Biol.* **2021**, *31* (10), R522−R529.
(32) Lehmann, L.; Soukup, S. T.; Gerhauser, C.; Vollmer, G.; Kulling, S. E. Isoflavone-containing dietary supplements. *Bundesgesundheitsblatt Gesundheitsforschung Gesundheitsschutz* **2017**, *60* (3), 305−313.
(33) Steen, K.; Chen, D.; Wang, F.; Majumdar, R.; Chen, S.; Kumar, S.; Lombard, D. B.; Weigert, R.; Zieman, A. G.; Parent, C. A.; Coulombe, P. A. A role for keratins in supporting mitochondrial organization and function in skin keratinocytes. *Mol. Biol. Cell* **2020**, *31* (11), 1103−1111.
(34) Sharma, S.; Conover, G. M.; Elliott, J. L.; Der Perng, M.; Herrmann, H.; Quinlan, R. A. alphaB-Crystallin is a sensor for assembly intermediates and for the subunit topology of desmin intermediate filaments. *Cell Stress Chaperones* **2017**, *22* (4), 613−626.
(35) Vaxman, I.; Gertz, M. When to Suspect a Diagnosis of Amyloidosis. *Acta Haematol.* **2020**, *143* (4), 304−311.
(36) Gupta, N.; Kaur, H.; Wajid, S. Renal amyloidosis: an update on diagnosis and pathogenesis. *Protoplasma* **2020**, *257* (5), 1259−1276.
(37) Lu, J.; Xu, H.; Xia, J.; Ma, J.; Xu, J.; Li, Y.; Feng, J. D- and Unnatural Amino Acid Substituted Antimicrobial Peptides With Improved Proteolytic Resistance and Their Proteolytic Degradation Characteristics. *Front Microbiol* **2020**, *11*, No. 563030.
(38) Song, N.; Li, H.; Tang, Q.; Luo, S.; Shi, Z.; Zhao, Q.; Li, R.; Chen, Y.; Cai, X.; Jiang, X. Design and Discovery of Novel Cyclic Peptides as EDPs-EBP Interaction Inhibitors for the Treatment of Liver Fibrosis. *J. Med. Chem.* **2023**, *66* (7), 4689−4702.
(39) Dong, J.; Xiao, J.; Li, J.; Yu, H.; Zhao, Q.; Tang, Q.; Chen, H.; Liu, H.; Wu, K.; Lei, J.; Wang, R.; Jiang, X. Discovery and Design of Novel Cyclic Peptides as Specific Inhibitors Targeting CCN2 and Disrupting CCN2/EGFR Interaction for Kidney Fibrosis Treatment. *J. Med. Chem.* **2023**, *66* (12), 8251−8266.
(40) Wang, Y.; Xue, F.; Cheng, W.; Zhao, Q.; Song, N.; Shi, Z.; Liu, H.; Li, Y.; Tang, Q.; Liu, Q.; Wang, Y.; Zhang, F.; Jiang, X. Design and Synthesis of Novel Ultralong-Acting Peptides as EDP-EBP Interaction Inhibitors for Pulmonary Fibrosis Treatment. *J. Med. Chem.* **2024**, *67* (8), 6624−6637.
(41) Liu, X.; Li, M.; Chen, Z.; Yu, Y.; Shi, H.; Yu, Y.; Wang, Y.; Chen, R.; Ge, J. Mitochondrial calpain-1 activates NLRP3 inflammasome by cleaving ATP5A1 and inducing mitochondrial ROS in CVB3-induced myocarditis. *Basic Res. Cardiol* **2022**, *117* (1), 40.
(42) Ikeda, G.; Santoso, M. R.; Tada, Y.; Li, A. M.; Vaskova, E.; Jung, J. H.; O'Brien, C.; Egan, E.; Ye, J.; Yang, P. C. Mitochondria-Rich Extracellular Vesicles From Autologous Stem Cell-Derived Cardiomyocytes Restore Energetics of Ischemic Myocardium. *J. Am. College Cardiol.* **2021**, *77* (8), 1073−1088.
(43) Liu, T.; Sun, L.; Zhang, Y.; Wang, Y.; Zheng, J. Imbalanced GSH/ROS and sequential cell death. *J. Biochem. Mol. Toxicol.* **2022**, *36* (1), No. e22942.
(44) Xiao, Y.; Zhang, T.; Ma, X.; Yang, Q. C.; Yang, L. L.; Yang, S. C.; Liang, M.; Xu, Z.; Sun, Z. J. Microenvironment-Responsive Prodrug-Induced Pyroptosis Boosts Cancer Immunotherapy. *Adv. Sci.* **2021**, *8* (24), No. e2101840.
(45) Zhao, X.; Wang, Y.; Zhu, T.; Wu, H.; Leng, D.; Qin, Z.; Li, Y.; Wu, D. Mesoporous Calcium-Silicate Nanoparticles Loaded with Prussian Blue Promotes Enterococcus Faecalis Ferroptosis-Like Death by Regulating Bacterial Redox Pathway ROS/GSH. *Int. J. Nanomedicine* **2022**, *Volume 17*, 5187−5205.
(46) Loeff, D. S.; Filler, R. M.; Vinograd, I.; Ein, S. H.; Williams, W. G.; Smith, C. R.; Bahoric, A. Congenital tracheal stenosis: a review of 22 patients from 1965 to 1987. *J. Pediatr Surg.* **1988**, *23* (8), 744−748.

https://doi.org/10.1021/acsomega.4c10956
ACS Omega 2025, 10, 9661−9674